Conf-940707--1

UCRL-JC- 118297
PREPRINT

Experiments with highly charged ions up to bare U^{92+} on the electron beam ion trap

Peter Beiersdorfer

This paper was prepared for submittal to the
Proceedings of the 14th International Conference on Atomic Physics
Boulder, CO
July 31-August 5, 1994

July 1994

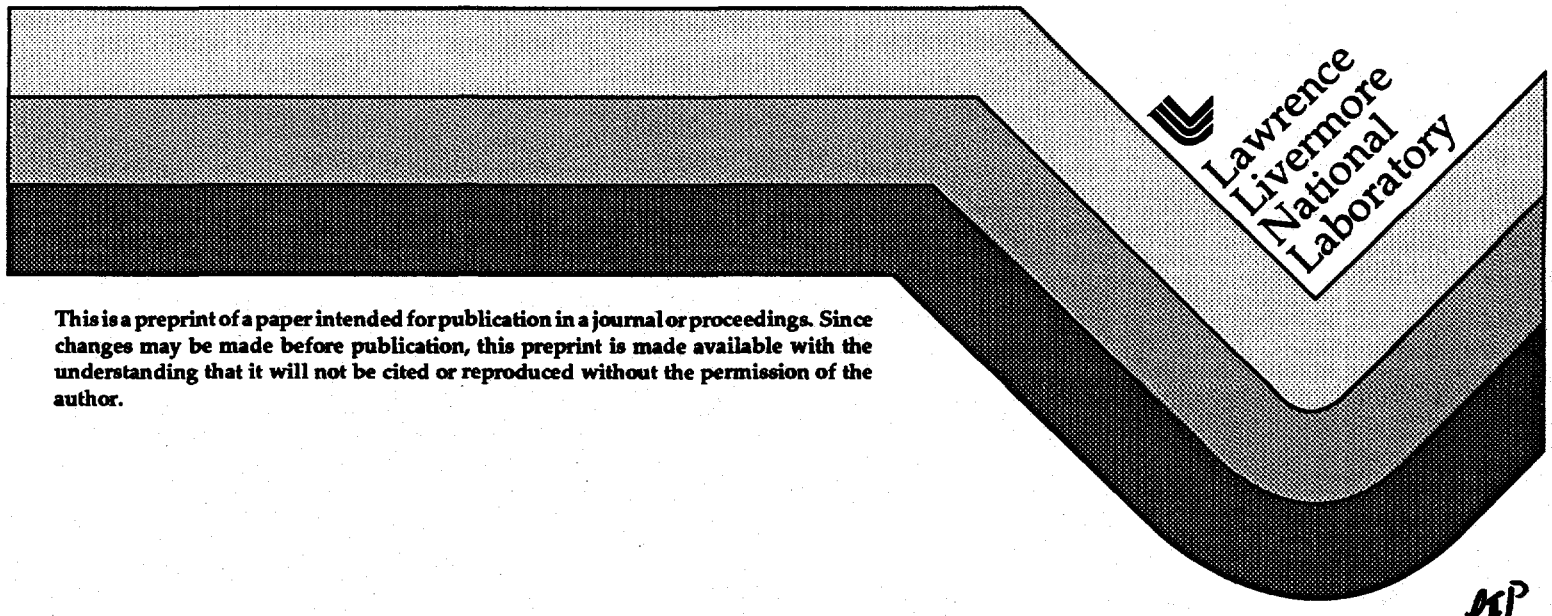

LSP

Experiments with highly charged ions up to bare U^{92+} on the electron beam ion trap

Peter Beiersdorfer
Lawrence Livermore National Laboratory
Livermore, CA 94551

Abstract

An overview is given of the current experimental effort to investigate the level structure of highly charged ions with the Livermore electron beam ion trap (EBIT) facility. The facility allows the production and study of virtually any ionization state of any element up to bare U^{92+}. Precision spectroscopic measurements have been performed for a range of $\Delta n = 0$ and $\Delta n = 1$ transitions. Examples involving 3–4 and 2–3 as well as 3–3 and 2–2 transitions in uranium ions are discussed that illustrated some of the measurement and analysis techniques employed. The measurements have allowed tests of calculations of the the quantum electrodynamical contributions to the transitions energies at the 0.4% level in a regime where $(Z\alpha) \approx 1$.

I. Introduction

The strong nuclear field of high-Z, highly charged ions provides an ideal environment for measuring the nonperturbative aspects of QED theory where $(Z\alpha) \approx 1$. This is especially true for the contributions from the electron self-energy. The self-energy contribution cannot be tested in high-Z muonic atoms, and higher order terms in $(Z\alpha)$ are too small in low-Z multi-electron ions and cannot be measured relative to the size of the uncertainties in solving the Schroedinger equation.

Highly charged, high-Z ions have been produced in a variety of sources. In tokamaks and high-power laser-produced plasmas the highest attainable charge state of uranium, the highest-Z naturally occurring element, approaches that of nickellike U^{64+}. Yet higher charge states, have been produced in heavy-ion accelerators, as attested by two recent measurements of the K-shell transitions in hydrogenlike and heliumlike uranium [1,2]. While accelerators combined with storage-ring facilities can now provide virtually any ion imaginable, the experimental conditions are very challenging. Ions are moving at relativistic speeds, and there typically is a high-radiation environment. As a result, only two other spectroscopic measurements of very highly charged uranium ions have been reported apart from the two measurements already mentioned. These are the measurements of the $2s_{1/2}$–$2p_{1/2}$ energy splittings in lithiumlike U^{89+} [3] and in heliumlike U^{90+} [4].

During the past six years the electron beam ion trap (EBIT) has been operated as a spectroscopic source at the Lawrence Livermore National Laboratory. Like ion-beam accelerator facilities it also is able to produce very highly charged ions. This included ions as highly charged as neonlike U^{82+} [5]. Recently, a high-energy version, dubbed Super-EBIT, started operation. This machine has produced ions as highly charged as bare U^{92+} [6]. Unlike accelerator sources, the ions in EBIT are stationary and trapped in the space-charge potential of the electron beam. Their thermal temperature was shown to be less than a few hundred eV [7]. As spectroscopic sources the EBIT devices thus use the inverse of the accelerator-based beam-foil or beam-gas jet technique. Instead of a stationary electron target interacting with relativistic ions, the ions in

EBIT form a stationary target interacting with a relativistic electron beam. Under these conditions, "standard" spectroscopic techniques can be applied to measuring the emission from highly charged ions [8], and systematic measurements over a wide range of ions and transitions are possible.

Experiments on EBIT so far include high-resolution crystal spectrometer measurements of the x-ray emission from M-shell transitions in nickellike U^{64+} and L-shell transitions in neonlike U^{82+}, as well high-resolution crystal spectrometer measurements of $3s_{1/2}$–$3p_{3/2}$ transitions in near sodiumlike and of $2s_{1/2}$–$2p_{3/2}$ transitions in near heliumlike uranium. Moreover, measurements of K-shell transitions have been made with solid-state detectors that prove the production of hydrogenic and lithiumlike uranium. The relatively easy access to highly charged ions and the precision achieved in these measurements, which rivals and exceeds that of other source, indicates that experimental atomic physics has finally entered an era, where all ions of all elements in the periodic table are accessible to scrutiny.

In the following, we present an overview of spectroscopic measurements of highly charged ions using the EBIT facility. We discuss the focus of our current research effort, and we illustrate some of the measurements and analysis techniques employed. In doing so we use experiments involving uranium as examples. The range of elements studied on EBIT, however, spans virtually all elements starting from oxygen.

II. The EBIT Device

EBIT uses an electron beam to generate, trap, and probe very highly charged ions [9]. The ion trap is kept short (≤ 4 cm) to minimize instabilities, which might affect the electron beam and reduce the maximum achievable charge state. The electron beam passing through the trap is compressed to a radius of about 30 μm by a 3-T magnetic field generated by a pair of superconducting Helmholtz coils. Six radial slots allow direct viewing of the trapped ions in a plane perpendicular to the electron beam.

Neutrals or ions are injected into the trap from a metal vapor arc [10] or through a gas

valve. Typically, the trapping region contains about 50,000 ions, i.e., the ion density is about 10^9 cm^{-3}. By contrast, the electron density is around 5×10^{12} cm^{-3}. Hence, the trap operates in a low-collisional regime, and metastable ions do not affect the operation under most circumstances.

Because collisions with the electron beam results in the heating of the ions, light-ion cooling is used to prevent detrapping of heavy ions [11]. For this purpose a low-Z gas, such as nitrogen, is introduced to the trap to spoil the high vacuum. Fully stripped nitrogen (N^{7+}) or neon (Ne^{10+}) can escape the trap much more readily than, for example, neonlike uranium (U^{82+}). As light ions leave the trap, they carry away heat and thus prevent the build-up of ion temperatures sufficient to detrap heavy ions. Trapping times of up to 4 hours were observed for neonlike gold with light-ion cooling [12]. Without cooling the observed trapping time is only a few seconds. A measurement of the ion temperature was performed recently showing that temperature at least as low as 100 eV can be achieved [7].

Super-EBIT functions almost identically to EBIT. However, modifications to the electron gun and collector assembly allow the use of electron beams with energies exceeding 200 kV [12].

III. Spectroscopic Instrumentation

Because EBIT was designed as an x-ray source, instrumentation emphasized x-ray detection and analysis. Solid-state detectors provide a highly efficient means for x-ray observation because of their near 100% quantum efficiency. Efficiency is especially important, as the number of photons produced in EBIT is low compared to plasma or beam-foil sources. Another advantage is their wide energy coverage. Crystal spectrometers provide much higher-spectral resolution than solid-state detectors. Their counting efficiency, however, is greatly reduced mainly because of low crystal reflectivities.

Because of the 50-μm width of its electron beam EBIT represents a line source. It is thus well suited for the deployment of flat-crystal spectrometers in the von Hámos geometry. The von Hámos geometry provides focusing of x rays in the non-dispersive direction. As a result, its

efficiency surpasses that of a flat-crystal spectrometer [13], and, by employing large-radius crystals, very high resolving powers can be attained. Flat-crystal spectrometers, by contrast, are easier to operate and to align to different Bragg angles. A flat-crystal spectrometer that operates in vacuo was installed on EBIT just recently [14], complementing the set of von Hamos-type spectrometers that have been standard for many years [13].

IV. Measurements of Near-Nickellike U^{64+}

The n=4 → n=3 M-shell transitions span a wide energy band from about 2.5 to 4.5 keV in uranium. A survey of the M-shell emission on EBIT was made with a Si(Li) detector and a low-resolution flat-crystal spectrometer by DelGrande et al [15]. Much higher resolution was achieved in subsequent measurements. In particular, a measurement that achieved a precision of 80 ppm enabled the first identification of magnetic octupole decay in an atomic system [16].

The first excited level in the closed-shell lithiumlike ion, the level $1s2s\ ^3S_1$, decays to the $^1S_0$ ground state via a magnetic dipole transition [17]. The lowest excited level in the closed-shell neonlike ion, the level $(2p^5_{3/2}\ 3s_{1/2})_{J=2}$, decays to the ground state via a magnetic quadruple transition [18]. Similarly, the first excited level in the closed-shell nickellike ion, the level $(2p^5_{3/2}\ 4s_{1/2})_{J=3}$, decays to the $^1S_0$ ground state via a magnetic octupole transition [16]. A high-resolution spectrometer is necessary to resolve this transition from neighboring electric quadruple transition from level $(3d^9_{3/2}\ 4s_{1/2})_{J=2}$ in nickellike U^{64+}, as illustrated in Fig. 1. Its wavelength was measured as 4.6103(3) Å; that of the neighboring electric quadruple transition was measured to be 4.6058(3) Å.

In Fig. 1 we also present a synthetic spectrum for comparison with the measurements. In many of our measurements we rely on such calculations to unambiguously identify observed features. The synthetic spectrum was constructed from line intensities calculated with a detailed collisional-radiative model that incoporates wave functions, energy levels, and radiative transitions rates calculated by using the relativistic, multi-configuration parametric potential method with full configuration interaction [19]. The collisional excitation rates were calculated in

the distorted-wave approximation. For this an efficient technique, which performs an angular factorization of both the direct and exchange contributions to excitation cross sections and interpolates the necessary radial integrals as a function of threshold energy [20] was used. The resulting model includes all singly excited levels with a $3s^{-1}$, $3p^{-1}$, or $3d^{-1}$ core and an optical electron in the n=4 or 5 shell. Level populations are calculated from a balance of all radiative transitions and electron-impact excitations connecting these levels, of which there are more than 40 000. The model predicts that electron collisions do not affect the population of these excited levels for electron densities below about 10^{14} cm^{-3}. Moreover, the low-lying excited levels are not populated by direct electron-impact excitation from the ground state. Instead, they are populated almost exclusively by radiative cascades form higher levels. Direct electron collisions contribute to the excitation of the $(3d_{5/2}^{-1}4s)_{J=3}$ level, for example, less than 1%. By contrast, radiative cascade feeding from high-lying levels, involving many intermediate levels, is highly effective in populating the J=3 level, making the $M3$ line the sixth most intense line in the nickel-like M-shell spectrum.

V. Measurements of Near-Neonlike U^{82+}

The n=3 → n=2 L-shell transitions in neonlike U^{82+} are situated in the energy band 12-19 keV. The observation of such transitions thus requires spectrometers that can operate efficiently at small Bragg angles.

Recently, we have implemented a von Hámos-type spectrometer that employed a detector with high quantum efficiency for photon energies exceeding 10 keV [21]. This allowed us, for example, to measure the electric dipole and magnetic quadruple transitions from levels $(2p^5{}_{3/2}\ 3s_{1/2})_{J=1}$ and $(2p^5{}_{3/2}\ 3s_{1/2})_{J=2}$ to ground, respectively, as shown in Fig. 2 (a). These lines were recorded in second order Bragg reflection. The wavelengths of these lines are determined relative to the wavelength of the Lyman-α lines in manganese measured in first order, whose energies are given by Johnson and Soff [22]. Similar use of hydrogenic reference lines is used in virtually all of our crystal-spectrometer measurements. A spectrum of the manganese

transitions is shown in Fig. 2(b). We find 12,877.20(80) eV for the electric dipole and 12,866.07(90) eV for the magnetic quadruple transition. As the comparisons with theoretical values in Table I shows, there is a significant difference with relativistic calculations employing a multiconfiguration Dirac-Fock (MCDF) code [23]. The disagreement might be caused by correlation effects as well as by inaccurate estimates of the QED terms from a semi-empirical scaling of hydrogenic values [24]. We discuss these possibilities in more detail in the next section.

The relative contribution of QED to the transition energy is enhanced, if we study 3s–3p transitions instead of 2p–3s transitions. Such transitions can be studied most readily in charge states lower than neonlike, especially in sodiumlike and magnesium-like ions. With the help of many-body perturbation theory, it is now possible to calculate the Dirac energies of one-valence-electron ions, such a sodium like ions, with very high precision [25]. In contrast to neonlike ions, where the calculated Dirac energies are not yet known with high precision, the QED terms in sodiumlike ions can be isolated from the non-QED terms and measurements thus directly compared to QED calculations by subtracting off the Dirac energies.

The $3s_{1/2}$–$3p_{3/2}$ transitions in high-Z ions fall into the energy region from about 800 eV for lead to 1100 eV for uranium. To measure such low-energy transitions vacuum spectrometers are necessary. We have recently implemented such a spectrometer on EBIT [14] and made a preliminary measurement of the $3s_{1/2}$–$3p_{3/2}$ transitions in near sodiumlike lead. The result is shown in Fig. 3. The spectrum was recorded for only one hour of observation time, but clearly showed features from sodiumlike, magnesiumlike, aluminumlike, and siliconlike lead. As in the case of the uranium M-shell spectra, a detailed collisional-radiative model was constructed to aid in the analysis. Results from an energy determination of the observed lines are given in Table II.

Despite the short observation time our measurement is already comparable in accuracy to a much more elaborate measurement of 3–3 transitions in Na-like Pb performed on the Unilac accelerator facility and reported very recently [26]. The Unilac measurement reported 798.65±0.13 eV for a blend of the Na-like 3s–3p transition and several Ne-like transitions,

which is in agreement with our value of 789.92±0.26 eV. The QED contributions to this transition are calculated to be 6.46 eV [26] so our measurement represents a 4%-test of these calculations. An extension of our 3–3 measurement to near-sodiumlike uranium ions is planned for the near future.

VI. Measurements of Near-Heliumlike U^{90+}

QED terms scale approximately as n^{-3}, where n is the principal quantum number. The QED contribution to a transition involving a 4s electron in near-nickellike U^{64+} is about 3eV, while it is about 10eV for transitions involving a 3s electron, about 42eV for those involving a 2s electron, and about 460 eV for K-shell transitions. As a percentage of the transition energy QED effects are largest for $\Delta n = 0$ intrashell transitions in the $n = 2$ shell. Although the L-shell QED energies are more than eight times smaller, the Dirac energies are at least 25-fold smaller than in the case of K-shell transitions. For this reason, we have initially concentrated on measuring $n = 2 \rightarrow 2$ transitions [27]. A high-resolution spectrum of the $2s_{1/2}$–$2p_{3/2}$ transitions in lithiumlike U^{89+} through neonlike U^{82+} is shown in Fig. 4. Nevertheless, measurements of the QED contributions to the uranium 1s electron are in progress [28] and promise to provide very high precision results.

In recording the $2s_{1/2}$–$2p_{3/2}$ transitions the ionization balance in the trap was varied by changing the electron energy, the neutral gas density (i.e., the charge-exchange recombination rate), and the effective current density [27]. This allowed a study of the full range of charge states from U^{82+} to U^{89+}. The beam energies used were well above the 33-keV ionization potential of lithiumlike U^{89+} and below the 130-keV ionization potential of heliumlike U^{90+}. As a result, we observed and unequivocally identified the features produced by all thirteen $2s_{1/2}$-$2p_{3/2}$ electric dipole transitions from the eight ionization stages U^{82+} through U^{89+} that were predicted to fall in our spectral region [27].

From these measurements we determined 4459.37±0.35 eV for the $2s_{1/2}$-$2p_{3/2}$ transitions in lithiumlike U^{89+} with a 90% confidence level [27]. More recently, we measured

the $2s_{1/2}$–$2p_{3/2}$ transition in lithiumlike Th^{87+} through neonlike Th^{80+} [29]. Here, the $2s_{1/2}$ –$2p_{3/2}$ transitions in lithiumlike Th^{87+} was determined to be 4025.14±0.14 eV at a 1-σ confidence level.

The measurements of lithiumlike U^{89+} and Th^{87+} are in excellent agreement with recent *ab initio* calculations of the QED energies [30] and represent a check of these calculations at the 0.4% level, i.e., a check with 10-times higher accuracy than that achieved in the 3–3 measurements. The agreement with theory is illustrated in Fig. 5, where we have plotted the fractional difference between measured and calculated QED contributions to the $2s_{1/2}$-$2p_{3/2}$ transitions in lithiumlike ions.

The $2s_{1/2}$–$2p_{3/2}$ transition measurements in berylliumlike U^{88+} through neonlike U^{82+} allows us to test relativistic correlation energies and QED calculations in highly charged ions with more than one valence electron. Comparing our measured transition energies to values computed with standard multi-configuration Dirac-Fock (MCDF) calculations, we find that such calculations significantly overestimate the transition energies, as illustrated in Fig. 6. The discrepancy increased with the number of spectator electrons in the $n = 2$ shell and can be attributed to residual correlation energies unaccounted for by the atomic structure calculations. This is true for both measurements thorium and uranium. Recently, efforts have been initiated that attempt to apply the principles of many-body perturbation theory to the calculations of the Dirac energies of such systems with more than one valence electron [31]. If successful, the Dirac energies of ions with more than one valence electron can be calculated with a precision now reserved for ions with a single valence electron. This would enable isolating the QED contributions and the development and testing of *ab initio* calculations of the QED terms for such ions.

VII. Conclusion

A vigorous, world-wide effort is currently under way to perform precise measurements of the atomic structure of highly charged, high-Z ions. At the Livermore EBIT facility this effort ranges from crystal-spectrometer measurements of near nickellike U^{64+} to measurements of the 1s-binding energy of hydrogenic U^{91+}. The large number of measurements in turn have spurred the development of formalisms to accurately calculate the Dirac and QED energies of any type of highly charged high-Z ion. In many cases, such calculations were impossible and unneeded just a few years ago.

In the case of those ions with one valence electron the measurements have provided precise values of the electron self-energy contribution to the level energies. Tests on the 0.4-% level of the total QED contribution were possible in a regime where $(Z\alpha) \approx 1$.

While our discussion so far has focused on measurements of atomic structure, experiments have also been performed that centered on others aspects of atomic physics. These included the measurement of the 1s-ionization cross sections of heliumlike U^{90+} and hydrogenic U^{91+}, which were found to be twice the size predicted by recent theory, and the first observation of quantum interference of radiative and dielectronic recombination in berylliumlike U^{88+} and boronlike U^{87+} [31]. These measurements demonstrate that experiments involving very highly charged ions are merely in their infancy and much work needs to be done.

Acknowledgments

The continued support of Mark Eckart and Andrew Hazi is greatly appreciated. This work was performed under the auspices of the U.S. Department of Energy by Lawrence Livermore National Laboratory under contract No. W-7405-ENG-48.

References

[1] J. P. Briand, P. Chevallier, P. Indelicato, K. P. Ziock, and D. Dietrich, Phys. Rev. Lett. **65**, 2761 (1990).

[2] Th. Stöhlker, P. H. Mokler, K. Beckert, F. Bosch, H. Eickhoff, B. Franzke, M. Jung, T. Kandler, O. Klepper, C. Kozhuharov, R. Moshammer, F. Nolden, H. Reich, P. Rymuza, P. Spädtke, and M. Steck, Phys. Rev. Lett. **71**, 2184 (1993).

[3] J. Schweppe, A. Belkacem, L. Blumenfeld, N. Claytor, B. Feinberg, H. Gould, V. E. Kostroun, L. Levy, S. Misawa, J. R. Mowat, and M. H. Prior , Phys. Rev. Lett. **66**, 1434 (1991).

[4] C. T. Munger and H. Gould, Phys. Rev. Lett. **57**, 2927 (1986).

[5] P. Beiersdorfer, Nucl. Instrum. Methods **B56/57**, 1144 (1991).

[6] R. E. Marrs, S. E. Elliott, and D. A. Knapp, Phys. Rev. Lett. **72**, 4082 (1994).

[7] P. Beiersdorfer, V. Decaux, S. Elliott, K. Widmann, and K. Wong, Rev. Sci. Instrum. **66** (January 1995) (in press).

[8] P. Beiersdorfer *et al.*, in *UV and X-Ray Spectroscopy of Astrophysical and Laboratory Plasmas*, ed. by E. Silver and S. Kahn (Cambridge University Press, Cambridge, 1993), p. 59.

[9] R. E. Marrs and M. A. Levine and D. A. Knapp and J. R. Henderson, Phys. Rev. Lett. **60**, 1715 (1988).

[10] I. G. Brown, J. E. Galvin, R. A. MacGill, and R. T. Wright, Appl. Phys. Lett. **49**, 1019 (1986).

[11] M. B. Schneider, M. A. Levine, C. L. Bennett, J. R. Henderson, D. A. Knapp, and R. E. Marrs, in *International Symposium on Electron Beam Ion Sources and their Applications - Upton, NY 1988*, AIP Conference Proceedings No. 188, edited by A. Hershcovitch (AIP, New York, 1989), p. 158.

[12] D. A. Knapp, R. E. Marrs, S. R. Elliott, E. W. Magee, and R. Zasadzinski, Nucl. Instrum. Methods **A334**, 305 (1993).

[13] P. Beiersdorfer, R. E. Marrs, J. R. Henderson, D. A. Knapp, M. A. Levine, D. B. Platt, M. B. Schneider, D. A. Vogel, and K. L. Wong, Rev. Sci. Instrum. **61**, 2338 (1990).

[14] P. Beiersdorfer and B. J. Wargelin, Rev. Sci. Instrum. **65**, 13 (1994).

[15] N. K. Del Grande, P. Beiersdorfer, J. R. Henderson, A. L. Osterheld, J. H. Scofield, and J. K. Swenson, Nucl. Instrum. Methods **B56/57**, 227 (1991).

[16] P. Beiersdorfer, A. L. Osterheld, J. Scofield, B. Wargelin, and R. E. Marrs, Phys. Rev. Lett. **67**, 2272 (1991).

[17] H. R. Griem, Astrophys. J. **156**, L103 (1969).

[18] M. Klapisch, J. L. Schwob, M. Finkenthal, B. S. Fraenkel, S. Egert, A. Bar Shalom, C. Breton, C. de Michelis, and M. Mattioli, Phys. Rev. Lett. **41**, 403 (1978).

[19] M. Klapisch, Comput. Phys. Commun. 2, 239 (1971); M. Klapisch, J. L. Schwob, B. S. Fraenkel, and J. Oreg, Opt. Soc. Am. **61**, 148 (1977).

[20] A. Bar-Shalom, M. Klapisch, and J. Oreg, Phys. Rev. A **38**, 1773 (1988).

[21] D. Vogel, P. Beiersdorfer, V. Decaux, and K. Widmann, Rev. Sci. Instrum. **66** (January 1995) (in press).

[22] W. R. Johnson and G. Soff, At. Data Nucl. Data Tables **33**, 405 (1985).

[23] I. P. Grant, B. J. McKenzie, P. H. Norrington, D. F. Mayers, and N. C. Pyper, Comput. Phys. Commun. **21**, 207 (1980); M. H. Chen, private communication.

[24] P. Beiersdorfer, M. H. Chen, R. E. Marrs, and M. A. Levine, Phys. Rev. A **41**, 3453 (1990).

[25] W. R. Johnson, S. A. Blundell, and J. Sapirstein, Phys. Rev. A **38**, 2699 (1988).

[26] A. Simionovici, D. D. Dietrich, R. Keville, T. Cowan, P. Beiersdorfer, M. H. Chen, S. A. Blundell, Phys. Rev. A **48**, 3056 (1993).

[27] P. Beiersdorfer, D. Knapp, R. E. Marrs, S. R. Elliott, and M. H. Chen, Phys. Rev. Lett. **71**, 3939 (1993).

[28] R. E. Marrs, private communication (1994); contributed presentation this conference.

[29] P. Beiersdorfer *et al.*, in preparation.

[30] S. A. Blundell, Phys. Rev. A **47**, 1790 (1993).

[31] J. Sapirstein, private communication (1994); invited presentation this conference.

[32] D. A. Knapp, P. Beiersdorfer, M. H. Chen, D. Schneider, and J. H. Scofield, Phys. Rev. Lett. (submitted).

Tables

TABLE I. Comparison between theoretical and experimental energies of $3s \rightarrow 2p$ transitions ion in neonlike U^{82+}. The theoretical values were obtained with a multiconfigurational Dirac-Fock (MCDF) code [23]. $E_{Coulomb}$ is the relativistic Coulomb energy, E_{Breit} is the transverse Breit correction, E_{VP} is the vacuum polarization energy, E_{SE} is the self-energy, and E_{total} is the sum of the preceding columns. ΔE is defined as the difference between the experimental energies E_{meas} and E_{total}. All values are in eV.

Transitions	$E_{Coulomb}$	E_{Breit}	E_{VP}	E_{SE}	E_{total}	E_{meas}	ΔE
$(3s_{1/2} \rightarrow 2p_{3/2})J=1$	12897.8	-31.9	-4.4	10.5	12872.0	12877.2	5.8±0.8
$(3s_{1/2} \rightarrow 2p_{3/2})J=2$	12886.9	-32.8	-4.4	10.5	12860.1	12866.1	6.0±0.9

TABLE II. Summary of measured energies of $3s_{1/2}$–$3p_{3/2}$ transitions in sodiumlike through siliconlike Pb (in eV). Values in parentheses indicate the uncertainty in the last digit. Theoretical energies are from MCDF calculations [23].

Key	Ion	Transition	$E_{measured}$	E_{MCDF}
Si	Pb^{68+}	$(3s_{1/2}3p^2{}_{1/2}3p_{3/2})_{J=1}\rightarrow(3s^23p^2)_{J=0}$	806.87(16)	806.93
Al-1	Pb^{69+}	$(3s_{1/2}3p_{1/2}3p_{3/2})_{J=3/2}\rightarrow(3s^23p_{1/2})_{J=1/2}$	803.16(31)	803.37
Al-2	Pb^{69+}	$(3s_{1/2}3p_{1/2}p_{3/2})_{J=1/2}\rightarrow(3s^23p_{1/2})_{J=1/2}$	814.77 (21)	816.65
Mg	Pb^{70+}	$(3s_{1/2}3p_{3/2})_{J=1}\rightarrow(3s^2)_{J=0}$	810.78(11)	812.11
Na	Pb^{71+}	$3p_{3/2}\rightarrow3s_{1/2}$	798.92(26)	799.43

Figures

Figure 1 (a) Survey spectrum of the 3–4 x-ray transitions in the low-energy region from near-nickellike uranium ions obtained at an electron-beam energy of 9.2 keV. (b) Model spectrum which includes transitions from copperlike U^{63+} (uppercase letters), nickellike U^{64+} (lines $M3$ and $E2$), and cobaltlike U^{65+} (lowercase letters). The assumed charge balance is U^{63+}:U^{64+} :U^{65+} = 1:1:1. (c) High resolution spectrum of nickellike U^{64+} in the region 2660–2710 eV recorded at an electron-beam energy of 7.1 keV. The $E2$ and $M3$ transitions are clearly resolved. Also seen is an electric quadruple transition in copperlike U^{63+}, labeled D in (b).

Figure 2 High-resolution spectra of (a) the $2p_{3/2}$–$3s_{1/2}$ transitions in neonlike U^{82+}, recorded in second order Bragg reflection, and (b) of the associated calibration lines in hydrogenic Mn^{24+}, recorded in first order. The electric dipole (J=1) and magnetic quadruple (J=2) transitions are measured . Unlabeled features are from lower charge states.

Figure 3 Spectrum of the $3s_{1/2}$–$3p_{3/2}$ transitions in sodiumlike, magnesiumlike, aluminumlike, and siliconlike lead, Pb^{68+}–Pb^{71+}. The spectrum was recorded during a 57-minute interval with the beam energy and current set to 29 kV and 140 mA, respectively.

Figure 4 Crystal-spectrometer spectrum of the $2s_{1/2}$–$2p_{3/2}$ electric dipole transitions in U^{82+} through U^{89+}. Lines are labeled by the charge state of the emitting ion.

Figure 5 Difference between theory and experiment for the $2s_{1/2}$–$2p_{3/2}$ transition energy in the lithiumlike isoelectronic sequence expressed as a percentage of the theoretical QED energy. The thorium and uranium points are form SuperEBIT and represent 68% confidence limits.

Figure 6 Average difference between MCDF calculations and measured 2–2 transition energies for different charge states of thorium and uranium. The difference increases for the lower charge states due to difficulties in calculating the electron correlation terms.

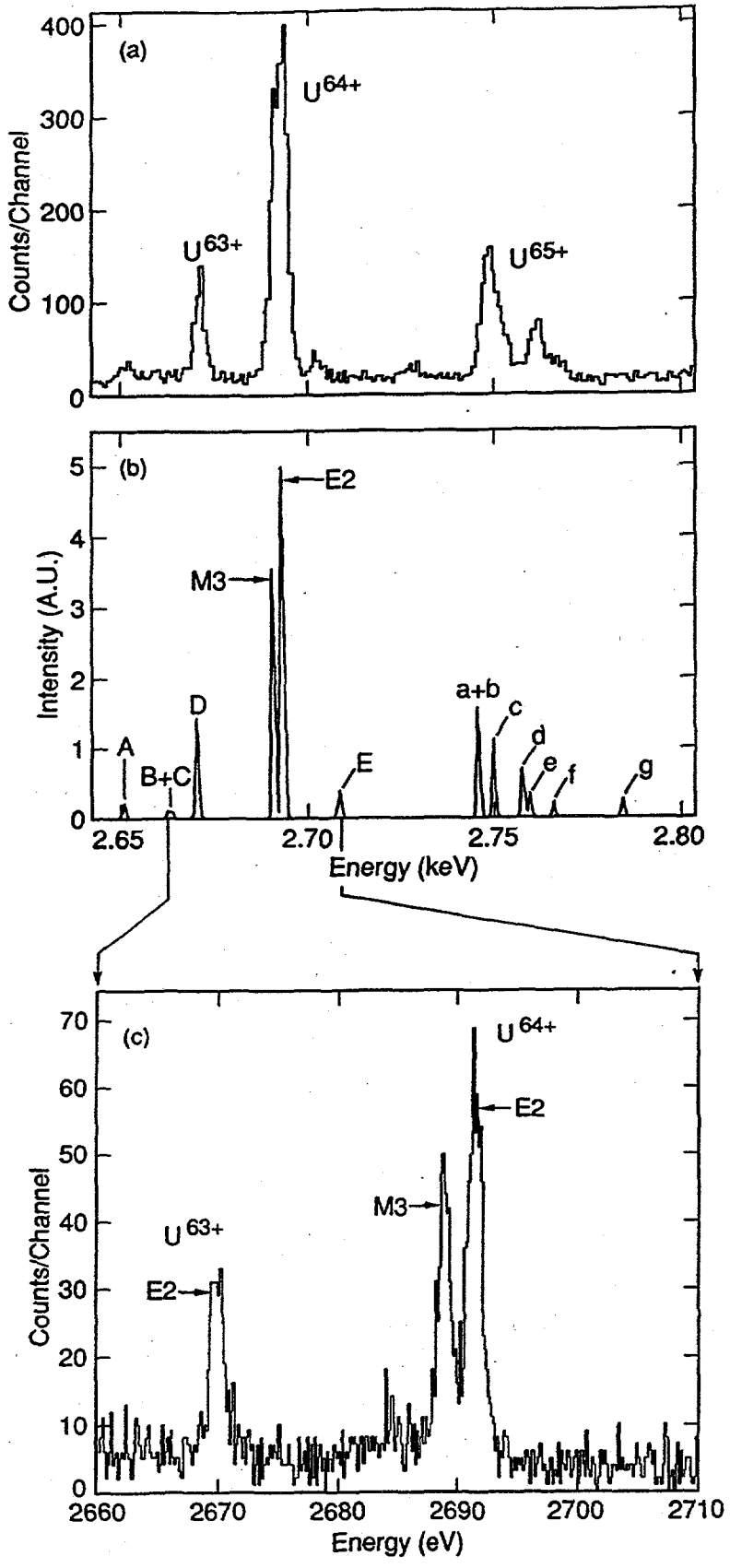
(a)
Counts/Channel
400
300
200
100
0
U64+
U63+
U65+
(b)
Intensity (A.U.)
5
4
3
2
1
0
E2
M3
A
B+C
D
E
a+b
c
d
e
f
g
2.65
2.70
2.75
2.80
Energy (keV)
(c)
Counts/Channel
70
60
50
40
30
20
10
0
U64+
E2
M3
U63+
E2
2660
2670
2680
2690
2700
2710
Energy (eV)

Figure 1.

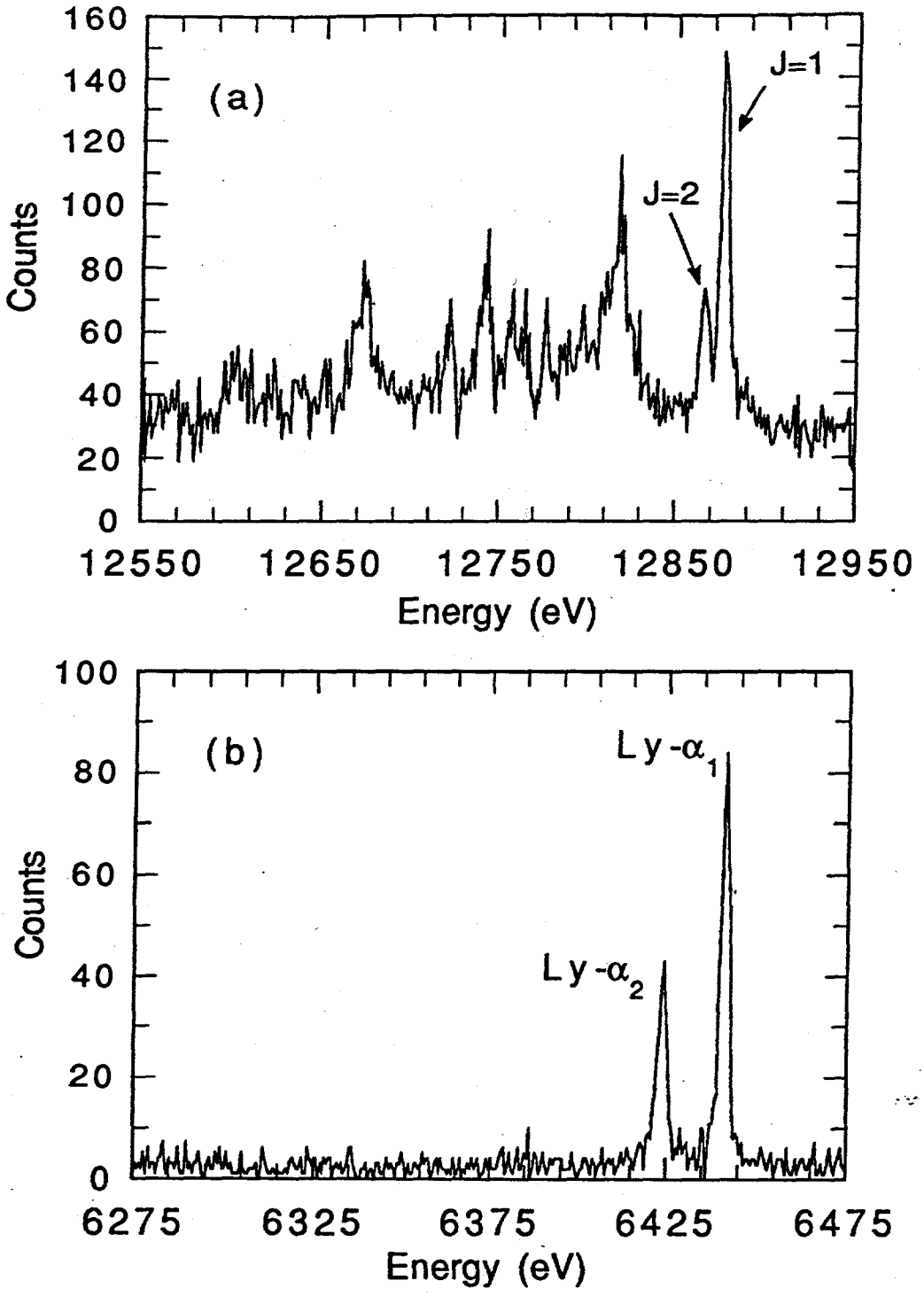
(a)
J=1
J=2
Counts
160
140
120
100
80
60
40
20
0
12550
12650
12750
12850
12950
Energy (eV)
(b)
Ly-α1
Ly-α2
Counts
100
80
60
40
20
0
6275
6325
6375
6425
6475
Energy (eV)

Figure 2.

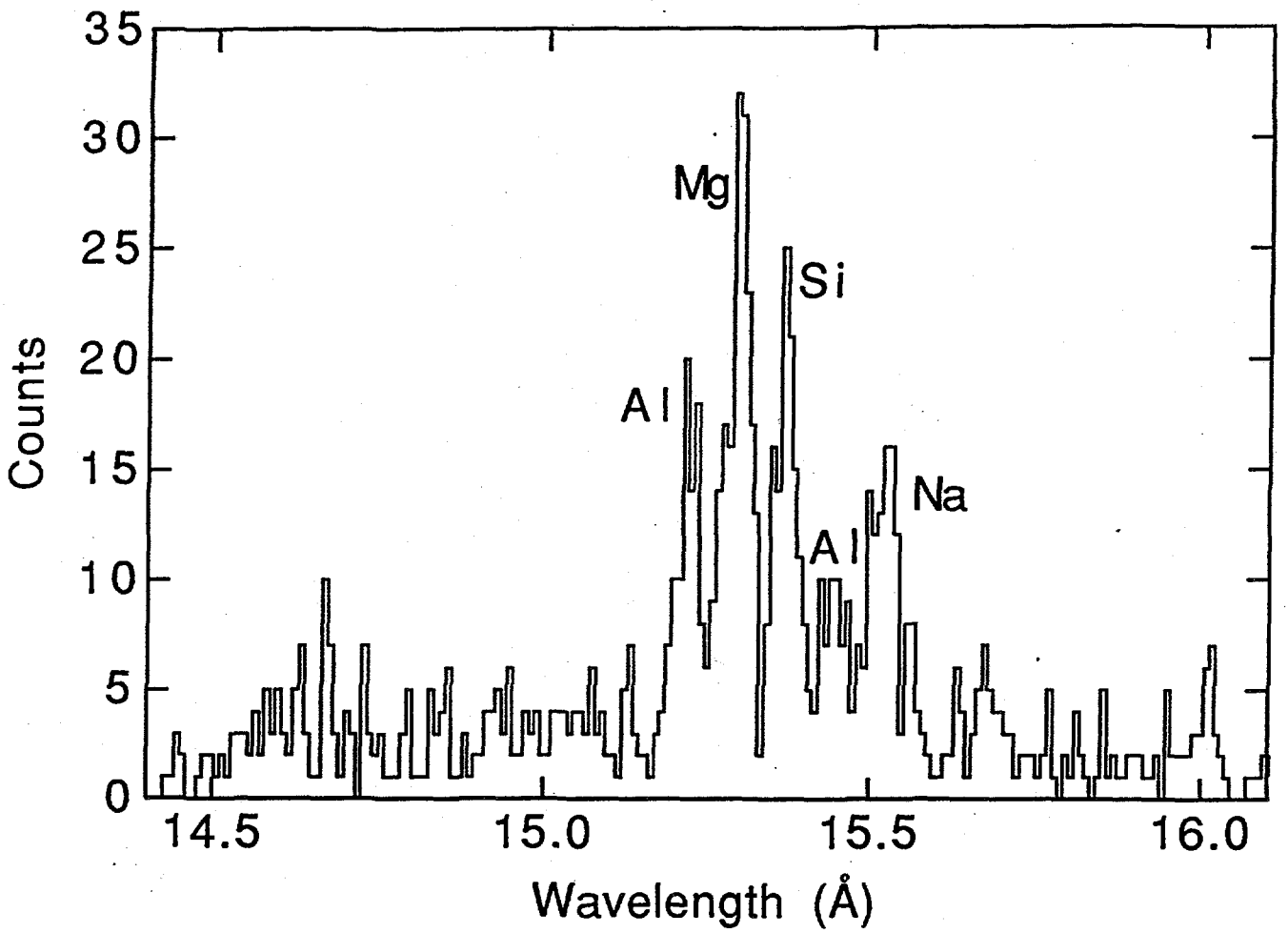
35
30
25
20
15
10
5
0
Counts
Mg
Si
Al
Al
Na
14.5
15.0
15.5
16.0
Wavelength (Å)

Figure 3.

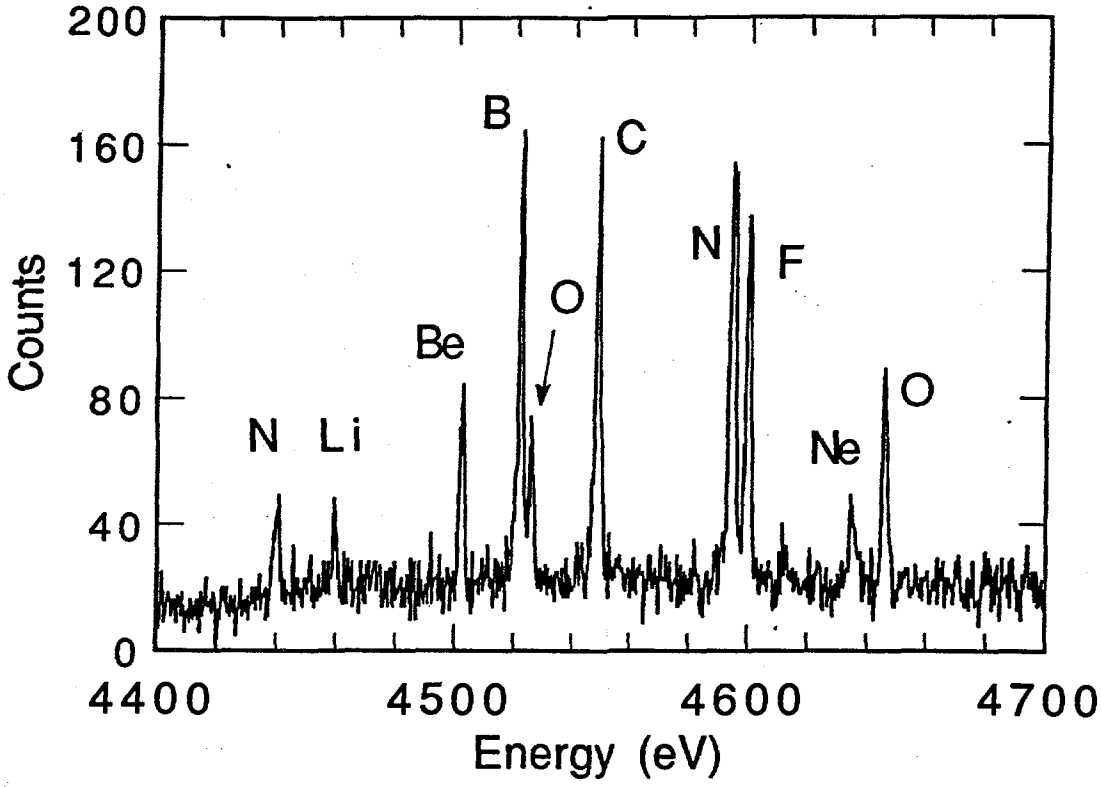
200
160
120
80
40
0
Counts
4400
4500
4600
4700
Energy (eV)
N
Li
Be
B
O
C
N
F
Ne
O

Figure 4.

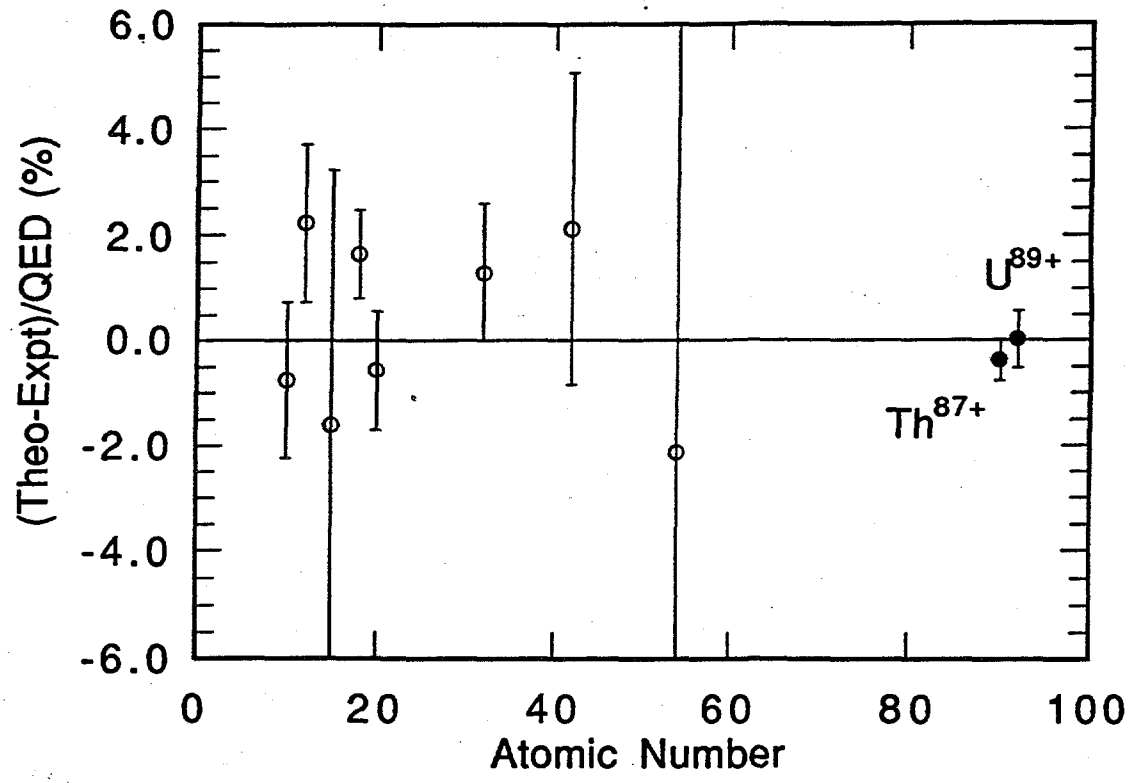
6.0
4.0
2.0
0.0
-2.0
-4.0
-6.0
(Theo-Expt)/QED (%)
0
20
40
60
80
100
Atomic Number
U89+
Th87+

Figure 5.

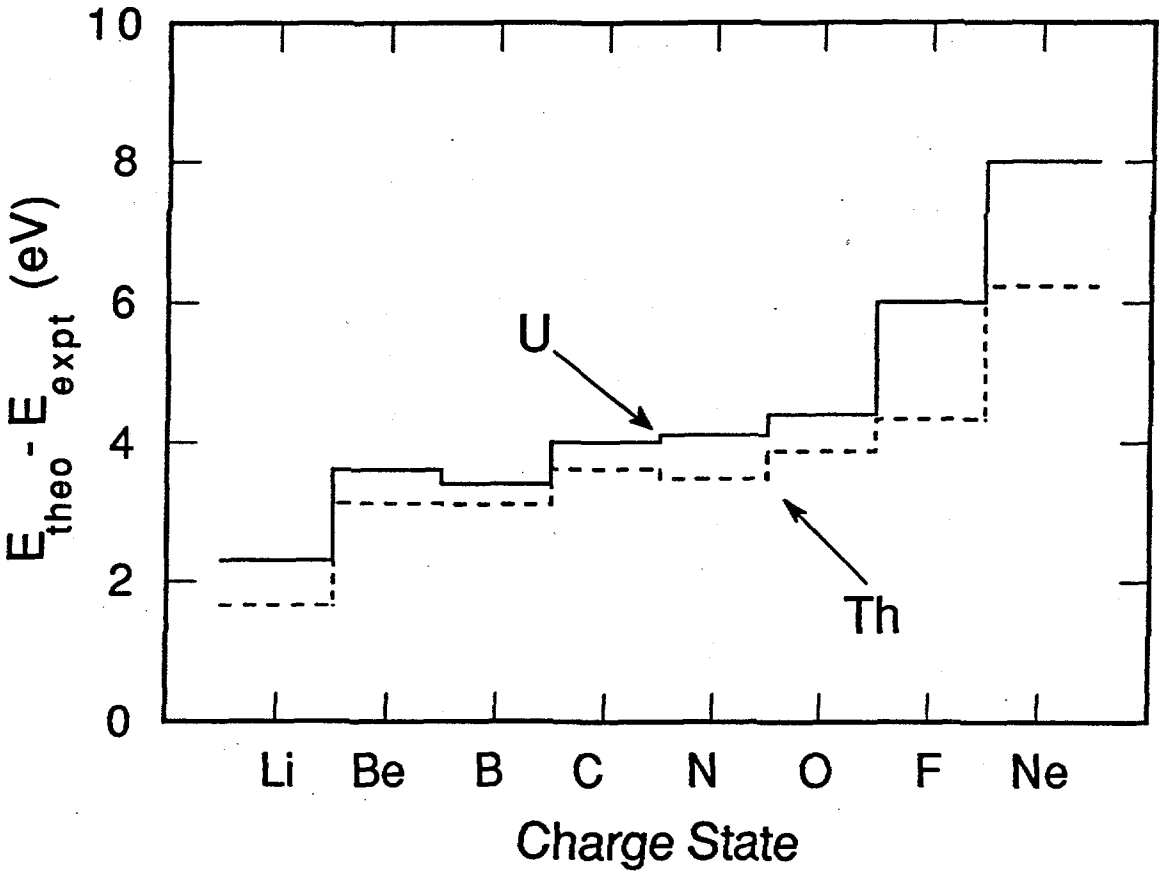

Figure 6.